Characterizing RNA dynamics at atomic resolution using solution-state NMR spectroscopy

Jameson R Bothe[1], Evgenia N Nikolova[2], Catherine D Eichhorn[2], Jeetender Chugh[3], Alexandar L Hansen[4–6] & Hashim M Al-Hashimi[1,3]

Many recently discovered noncoding RNAs do not fold into a single native conformation but sample many different conformations along their free-energy landscape to carry out their biological function. Here we review solution-state NMR techniques that measure the structural, kinetic and thermodynamic characteristics of RNA motions spanning picosecond to second timescales at atomic resolution, allowing unprecedented insights into the RNA dynamic structure landscape. From these studies a basic description of the RNA dynamic structure landscape is emerging, bringing new insights into how RNA structures change to carry out their function as well as applications in RNA-targeted drug discovery and RNA bioengineering.

Accompanying the discovery of noncoding RNAs (ncRNAs) as abundant players in gene expression and regulation is the growing realization that most ncRNA sequences do not fold into a single native conformation, but rather, ncRNAs sample many different conformations from their free-energy landscape[1,2] to carry out their biological function. For example, many ncRNAs function as genetic switches by transitioning between entirely different secondary structural forms in response to a wide range of cellular stimuli[3,4]. Not only do the structural characteristics of the different states have to be optimized to carry out distinct functions, transitions between them have to occur at dedicated timescales and be triggered by specific cellular signals. Thus, a deep molecular understanding of how ncRNAs perform their functions requires insights into how RNA dynamically samples different conformations along its energy landscape and how this landscape is in turn modulated by cellular cues[2].

Beyond understanding function, there are many reasons motivating studies of RNA dynamics at atomic resolution. First, RNA is exploding in its importance as a drug target[5], and a broader dynamic view of the conformations populating the energy landscape[1] is now widely recognized as essential for successfully implementing structure-based approaches in lead compound discovery and optimization[2,6]. Second, experimental data probing the dynamic aspects of RNA structure are urgently required for the continued testing and improvement of computational force fields, which remain severely underdeveloped for nucleic acids as compared to proteins[7]. Third, a predictive understanding of RNA dynamics will enable the design of RNA-based devices whose functionality often depends on dynamic transitions in structure.

The free-energy landscape[1] provides a unified and complete description regarding the dynamic properties of RNA that are relevant for understanding function (**Fig. 1**). The free energy is specified for every conformation that can be adopted by the RNA. The fractional population of a given conformer then depends on its relative free energy, whereas the rate at which two conformers interconvert depends on the free-energy barrier that separates them. Cellular cues perturb the free-energy landscape, diminishing barriers and/or stabilizing conformers that are otherwise

[1]Department of Chemistry, The University of Michigan, Ann Arbor, Michigan, USA. [2]Chemical Biology Doctoral Program, The University of Michigan, Ann Arbor, Michigan, USA. [3]Department of Biophysics, The University of Michigan, Ann Arbor, Michigan, USA. [4]Department of Chemistry, The University of Toronto, Toronto, Ontario, Canada. [5]Department of Biochemistry, The University of Toronto, Toronto, Ontario, Canada. [6]Department of Molecular Genetics, The University of Toronto, Toronto, Ontario, Canada. Correspondence should be addressed to H.M.A.-H. (hashimi@umich.edu).

PUBLISHED ONLINE 28 OCTOBER 2011; DOI:10.1038/NMETH.1735

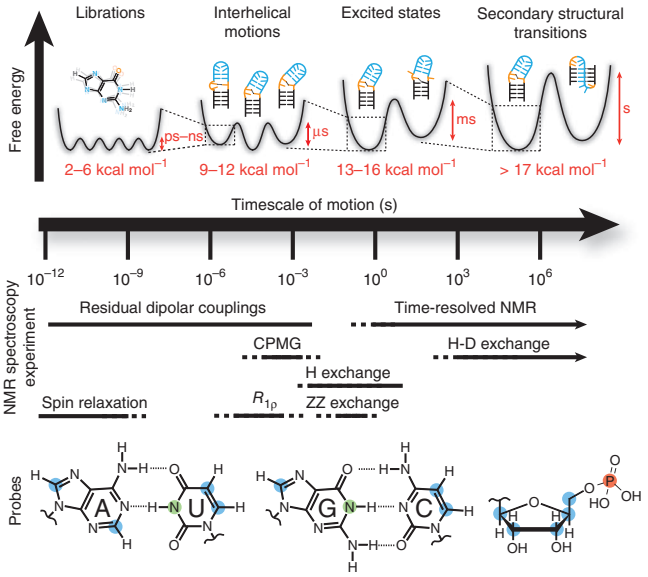

Figure 1 | NMR spectroscopy techniques and site-specific probes for characterizing motional modes that carry RNA structure along various regions of the dynamic structure landscape. In the dynamic structure landscape (top), transition free energies corresponding to typical timescales of interconversion were estimated using transition state theory at 25 °C. In NMR spectroscopy experiments (middle), solid lines indicate the timescales at which each NMR spectroscopy experiment is optimally suited for, and dashed lines indicate timescales that are difficult to probe. For probes (bottom), nuclei most commonly used for RNA dynamics measurements: protonated carbons (blue), imino nitrogens (green) and backbone phosphorus (red).

unfavorable, and thereby redistribute the conformer populations to effect specific biological outcomes. Although rich in information, the free-energy landscape is very complex and cannot be measured experimentally. Fortunately, important insights into biological function can be obtained by focusing on a subset of conformers that populate minima along the energy landscape. Studies increasingly show that such 'low-hanging fruit' conformers are often the ones that are stabilized by cellular cues to carry out biological function[8–10]. These more appreciably populated conformers are also more amenable to experimental characterization using spectroscopic techniques that probe dynamic fluctuations in structure along the energy landscape. We refer to this partial energy landscape as the 'dynamic structure landscape'.

Among many techniques that are now being developed to study RNA dynamics, solution-state NMR spectroscopy, which has also contributed considerably toward the characterization of protein dynamics[11], has a unique role (**Fig. 1**). First, NMR spectroscopy can be used to measure dynamics at atomic resolution, comprehensively for sugar, base and backbone moieties across different residues. Second, multiple interactions can be measured at a given site to deduce structural, kinetic and thermodynamic characteristics of not one but many motional modes occurring at different timescales. Third, NMR spectroscopy has broad sensitivity to motions spanning picosecond to second and longer timescales and can be used to characterize very subtle changes in conformation, including those involving minutely populated conformers (on the order of ~10^{-7}%) that have exceptionally short lifetimes (on the order of nanoseconds). Last but not least, NMR spectroscopy is a powerful approach for exploring how the dynamic structure landscape is modulated by cellular cues, and time-resolved methods can be used to follow these perturbations in real time.

Here we review solution-state NMR spectroscopy methods for studying RNA dynamics and highlight some of the new insights that have been obtained regarding the RNA dynamic structure landscape and its relationship to function.

Nuclear spin interactions used to study RNA dynamics

The basic NMR experiment can be simplistically described as follows. Nuclei behave as tiny magnets, and because of the quantization of the nuclear spin angular momentum, they align either parallel (α state) or antiparallel (β state) relative to the applied magnetic field. As the parallel (or antiparallel, depending on the nucleus) alignment is energetically more favorable, a net bulk magnetization over an ensemble of nuclei builds up parallel to the magnetic field. Radiofrequency pulses are then used to realign this bulk magnetization along a direction perpendicular to the magnetic field. The bulk magnetization then precesses about the magnetic field at a characteristic NMR frequency called the 'chemical shift' and gives rise to a detectable oscillating magnetic field. This non-equilibrium magnetization ultimately relaxes back to the equilibrium, parallel state. The time-domain spectrum is Fourier-transformed to yield the standard frequency-domain NMR spectrum, in which unique signals at characteristic chemical shift frequencies are observed for different types of nuclei. For nucleic acid applications, one is typically interested in the NMR-active nuclei ^{1}H, ^{13}C, ^{15}N, ^{2}H and ^{31}P. The ^{13}C, ^{15}N and ^{2}H isotopes can be introduced during synthesis, typically by using labeled NTPs via *in vitro* transcription reactions (**Fig. 1**).

The NMR chemical shift (**Box 1**) is proportional to the energy gap between the α and β states and the static applied magnetic field. However, electronic clouds surrounding nuclei can 'shield' or 'deshield' nuclei from the external magnetic field by variable amounts dependent on the electronic structure. This leads to a wide range of chemical shifts that makes it possible to measure dynamics with site-specific resolution. Furthermore, changes in chemical shift owing to local fluctuations in the electronic environment form the basis for relaxation dispersion experiments to measure exchange processes occurring at microsecond to millisecond timescales, ZZ-exchange spectroscopy to measure motions at millisecond to second timescales and time-resolved NMR spectroscopy experiments to follow transitions occurring at timescales longer than a few seconds.

In an NMR spectroscopy experiment, interactions such as dipolar coupling and chemical shift anisotropy (CSA) (**Box 1**) modulate the effective field experienced by a given nucleus in an orientation-dependent manner, thereby perturbing the energy gap between the α and β states and the observed NMR spectrum. Many NMR spectroscopy experiments that probe dynamics take advantage of these so-called 'anisotropic' interactions. In solution, the orientation dependence of anisotropic interactions gives rise to a time-dependent fluctuating field (**Fig. 2a**), which in turn influences the rate at which the magnetization relaxes back to equilibrium. The contribution to so-called transverse relaxation (R_2) is encoded within the linewidth of the NMR signal, with faster motions leading to narrower lines. Spin relaxation measurements take advantage of these effects to probe internal motions of bond vectors at picosecond to tens of nanosecond timescales.

BOX 1 BASIC NMR INTERACTIONS

Chemical shifts. Chemical shifts report on the local electronic environment surrounding nuclei and are highly sensitive to local geometry (for example, *syn* versus *anti* conformations, sugar puckers and others) and intermolecular interactions including hydrogen-bonding, stacking and metal interactions.

Scalar couplings (J-couplings). Scalar couplings arise from coupled interactions between the electron and nuclear spins of bonded nuclei that result in the splitting of NMR signals. Scalar couplings depend on the type of nuclei involved (typically larger for larger γ nuclei), number of bonds separating them (typically smaller the larger the number of bonds) and the dihedral angle in the case of three bond scalar couplings (^{3}J).

Dipolar couplings. The dipolar coupling between two nuclei i and j depends on $\gamma_i\gamma_j$ (γ values for ^{1}H, ^{13}C and ^{15}N follow the ratio 1.00:0.2515:–0.1014) and the inverse cubic distance (r_{ij}^{-3}) between the two nuclei. For relaxation, which is a second-order perturbation, this prefactor is squared, leading to a $\gamma^2\gamma^2r^{-6}$ dependence.

Chemical shift anisotropy. This interaction results from the anisotropic electronic environment, which 'shields' or 'deshields' nuclei from the external magnetic field in an orientation dependent manner. The chemical shift anisotropy contribution to spin relaxation scales quadratically with the external magnetic field and is usually less substantial than the dipolar interaction.

Though they influence relaxation, and thus the apparent linewidth of the NMR signal, anisotropic interactions average to zero owing to random tumbling of the molecule in solution and therefore do not affect the time-averaged effective field experienced by the nucleus and the observed time-averaged chemical shift frequency. However, these anisotropic interactions can be resurrected in solution by inducing a small degree of alignment, allowing the direct measurement of residual dipolar couplings (RDCs) and residual CSAs (RCSAs) (**Box 2**), which manifest as frequency offsets or added splittings when comparing unaligned and aligned samples, and can be used to probe motions at submillisecond timescales.

The above interactions form the basis for many of the NMR techniques used to probe nucleic acid dynamics that we review here. Note that although other types of NMR interactions, including nuclear Overhauser effect, rotating-frame Overhauser effect, scalar couplings and cross-correlated relaxation, can also be used to probe unique aspects of nucleic acid dynamics[12], they have so far primarily been used for structure determination and therefore we do not review them here.

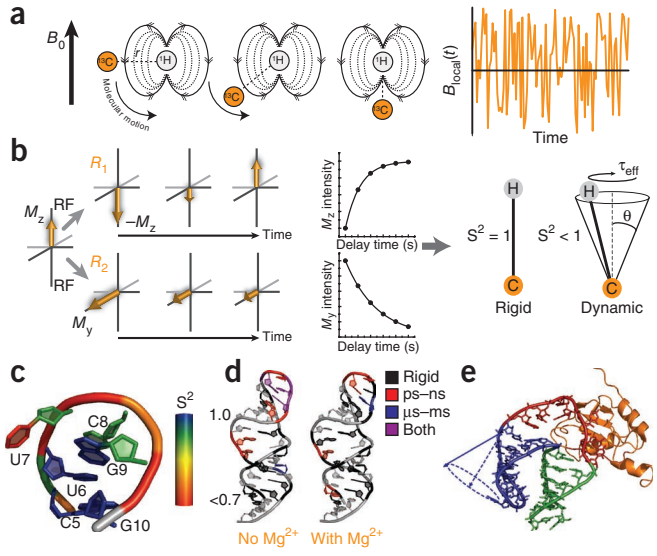

Sample preparation

NMR spectroscopy dynamics measurements, particularly those involving the measurement of picosecond to nanosecond motions by spin relaxation and microsecond to millisecond motions by relaxation dispersion, require the ability to isolate and measure specific interactions from what can be a complex network of interactions involving many nuclei. In general, unwanted NMR interactions increase with the gyromagnetic ratio (γ) of the nuclei involved, with decreasing distance of separation, and are difficult to suppress between nuclei of the same kind. Studies of protein dynamics have taken advantage of low γ backbone amide nitrogens, which have simple relaxation mechanisms. In nucleic acids, corresponding imino nitrogens (**Fig. 1**) are available for only guanines and uridines, and seldom in flexible residues of interest owing to rapid exchange of the imino protons with solvent. This has made it necessary to rely on carbon nuclei, which suffer from extensive ^{13}C-^{13}C interactions that complicate measurements and analysis of data, particularly for larger RNAs[13–16]. The preparation of NTPs with site-specifically labeled carbons helps isolate specific carbon nuclei, thus simplifying and in some cases enabling dynamics measurements that would otherwise be intractable. Examples of specific carbon labeling schemes that harness bacterial nucleotide biosynthetic pathways are shown in **Supplementary Table 1**.

Methods have also been developed to incorporate other types of nuclei with desirable spectroscopic properties. For example,

Figure 2 | Characterization of pico- to nanosecond motions using spin relaxation. (**a**) Reorientation of bond vectors leads to an oscillating local field, $B_{local}(t)$, at the nucleus of interest that influences relaxation. Shown is an example involving a ^{13}C-^{1}H dipolar interaction. (**b**) Model free analysis of longitudinal (R_1) and transverse (R_2) spin relaxation data yield an order parameter (S^2) describing the amplitude of motion and a constant (τ_{eff}) describing its timescale. RF, radiofrequency. (**c**–**e**) Example applications of spin relaxation in studies of RNA dynamics; site-specific U-U-C-G tetraloop dynamics (sugar and nucleobase order parameters[17,32] were determined at 298K whereas phosphate-backbone order parameters[18] were determined at 310K; **c**), redistribution of motional modes in the catalytic domain 5 RNA of a group II intron upon addition of Mg^{2+} (**d**; adapted from ref. 33 with permission from Elsevier), and RNA interhelical motions persist when bound to the human U1A protein (**e**; reprinted from ref. 39 with permission from the American Chemical Society).

BOX 2 THE NMR DYNAMICS TOOLKIT

Spin relaxation
Spin relaxation provides information about the amplitude and timescale of motions that reorient bond vectors (typically C-H and N-H) at picosecond to nanosecond timescales.

Pros. This approach provides both amplitude and timescale information for multiple motional modes occurring at different timescales involving the sugars, bases and phosphodiester backbone. There is an incredible potential wealth of information, the full scope of which has yet to be obtained by recording data at varying field strengths and for varying types of nuclei and interactions.

Cons. Contributions from overall motions can be difficult to quantitatively disentangle from those resulting from internal motions. Little information is typically obtained about the directionality of the motion, and fluctuations slower than overall tumbling can only partially be characterized. Complicating ^{13}C-^{13}C dipolar interactions grow substantially with increasing RNA size[13–16].

Residual dipolar couplings
This approach provides information about the amplitude of motions that reorient bond vectors (typically C-H and N-H) at timescales faster than ~10 milliseconds.

Pros. It can be measured in great abundance to probe dynamics of directly bonded and nonbonded internuclear vectors. It provides exquisite sensitivity to the orientation distribution of bond vectors spanning broad timescales and can be integrated with computational methods to steer molecular dynamics simulations or construct atomic-resolution ensembles. There is an incredible potential wealth of information, the full scope of which has yet to be obtained by recording data under different alignment conditions[49], using different frames of reference[54] and by exploiting motional couplings[48].

Cons. Contributions from overall motions can be difficult to quantitatively disentangle from those resulting from internal motions. Little to no information is obtained about motional timescales. This approach typically requires use of a potentially perturbing ordering medium and has limited sensitivity to small amplitude (<15°) motions.

Relaxation dispersion
Relaxation dispersion provides information about microsecond to millisecond transitions.

Pros. It can be used to characterize transitions to minutely populated excited state conformations (with populations of ~1–50%) that have very short lifetimes (hundreds of microseconds to 1 millisecond). Under favorable conditions, a complete thermodynamic and kinetic description of the transition can be obtained, along with the chemical shift of the excited state, which can be used to obtain insights into its structural features. There is an incredible potential wealth of information, which has yet to be obtained, by measuring RDC and RCSA–based relaxation dispersion for directly determining structures of excited states[96].

Cons. Chemical shift–based relaxation dispersion is only sensitive to conformational transitions that lead to changes in chemical shift. Analysis of data in terms of more than two states can be difficult and typically requires mutations to minimize the number of states. Data acquisition can be very time-consuming.

ZZ exchange
This approach provides rate information regarding transitions occurring at tens of milliseconds to ~1 s timescales.

Pros. It can be used to directly determine the forward and reverse rate constant for a transition under equilibrium conditions and is in principle not restricted to a particular atom type as in the H and H-D exchange. Recent methods developed for proteins might extend the sensitivity of ZZ-exchange experiments to highly skewed populations in RNA systems[100].

Cons. The exchanging species must be sufficiently populated (>30%) and exchange within a narrow window of timescales. If imino protons are used to probe exchange, the possibility of imino proton exchange with water during the mixing period should be considered.

Time-resolved NMR spectroscopy
This approach can be used to monitor a nonequilibrium state relax to equilibrium at timescales greater than a few seconds.

Pros. It can be used to dissect complex transitions involving multiple steps and different sites on a molecule. Kinetic initiation within the magnet with special hardware (laser or rapid mixing) allows for very short (~1–2 s) dead times. There is an incredible potential wealth of information which has yet to be obtained, for example, by measuring RDC and other NMR interactions in a time-resolved manner[73].

Cons. Without special hardware, mixing outside of the NMR magnet has long dead times (greater than ~20 s), thus reducing the time-sensitivity window. For laser initiation studies, chemical synthesis is required to attach photolabile groups to either small molecules or phosphoramidites. Laser-based studies are also limited by low sample concentrations to achieve full cleavage via short laser irradiation.

H and H-D exchange
This approach provides information regarding base-pair-opening kinetics and thermodynamics.

Pros. It can be used to probe exchange timescales over a broad range spanning 1 millisecond up to years. Data can be used to measure base-pair and open-state lifetimes as well as free-energy differences.

Cons. Experiments are limited to detectable imino and amino protons. H-D exchange experiments typically have dead times of ~3–5 min and cannot access base-pair open-state lifetimes and thermodynamics. H exchange assumes the exchange from the open state equals that of mononucleotides and neglects differences in accessibility and electrostatics.

deuterium has relatively simple relaxation mechanisms[17] that can be exploited in spin relaxation studies of pico- to nanosecond dynamics. RNA samples can be prepared using commercially available NTPs that are site-specifically deuterated at desirable ribose and/or nucleobase sites (**Supplementary Table 1**). Deuterated NTPs have also been used to simplify the spin relaxation mechanisms of ^{31}P as a unique probe of pico- to nanosecond backbone motions[18]. The site-specific introduction of ^{13}C labeled methyl probes has also been used to simplify the measurement and interpretation of ^{13}C based dynamics data and may potentially allow applications to much larger RNAs[19] (**Supplementary Table 1**).

Many NMR techniques for dynamics measurements, including spin relaxation and RDCs, probe the reorientation of bond vectors (C-H or N-H) relative to the external applied magnetic field. The ability to extract information regarding internal motions hinges on being able to disentangle these small spectroscopic contributions from the much larger contributions resulting from overall motions. Although this is typically accomplished by invoking the so-called 'decoupling approximation' and the assumption that internal and overall motions are not correlated to one another[20], studies increasingly show that the decoupling approximation breaks down in many flexible RNA systems[21–24]. Collective motions of helices can give rise to large changes in overall shape, and thus the overall motions, resulting in motional coupling that severely complicates data analysis. This problem was addressed with the introduction of a domain-elongation strategy[22] (**Supplementary Table 1**). In this approach, an RNA terminal helix is elongated using a stretch of isotopically unlabeled Watson-Crick base pairs designed to adopt an A-form helix structure. The resulting elongated RNA has an overall shape, and thus overall motions, that are far less sensitive to internal motions occurring in other parts of the molecule. Domain-elongation also broadens the time-scale sensitivity of spin relaxation data, expands the amount of RDC data that can be measured, and makes it possible to accurately compute RDC and spin relaxation data from molecular dynamics simulations.

Pico- to nanosecond motions from spin relaxation

Spin relaxation measurements (**Box 2**) of pico- to nanosecond motions take advantage of the fact that anisotropic interactions such as dipolar couplings and CSA (**Box 1**) modulate the effective field experienced by a given nucleus in an orientation-dependent manner, thus influencing the rate at which the bulk magnetization relaxes back to equilibrium. Let us consider how the dipolar interaction between a carbon and proton nucleus in a C-H bond modulates the effective magnetic field at the carbon nucleus (**Fig. 2a**). The carbon nucleus experiences both the static external magnetic field and the much smaller (~10^{-4}) magnetic field generated by the proton nucleus. Because the nuclear bar magnets are always quantized parallel (or antiparallel) to the magnetic field, the proton field experienced by the carbon nucleus will vary as the C-H bond changes orientation relative to the magnetic field, either because of internal or overall motions; in some orientations the proton field adds to the external magnetic field, in other orientations it subtracts or has no contribution (**Fig. 2a**). In the case of CSA, electrons oppose the magnetic field in a manner dependent on the orientation of the molecule relative to the field. As a result, internal and overall motions give rise to an oscillating magnetic field (**Fig. 2a**) at the carbon nucleus with a frequency comparable to the NMR transition frequency, thus stimulating relaxation. Note that internal motions occurring at timescales slower than overall motions will have only a small effect on the fluctuating field because the molecule will reorient many times before the internal motion has any effect. As a result, spin relaxation data are much less sensitive to motions occurring at timescales much slower than overall tumbling and is best suited for measuring dynamics on the picosecond to tens of nanosecond timescales, depending on the size of the nucleic acid.

Typically R_1 and R_2 relaxation rates (**Fig. 2b**) are measured together with heteronuclear nuclear Overhauser effect (a measure of the rate at which proton magnetization transfers to the heteronucleus owing to the dipolar interaction), and the data are analyzed using the model-free formalism[20], which yields an order parameter (S^2) describing the amplitude of motion of the C-H or N-H bond vector, ranging between 0 and 1 for maximum and minimum disorder, respectively, and a time constant (τ_{eff}) describing the rate of internal motions (**Fig. 2b**). More sophisticated models can be used to obtain amplitude and time constants for many distinct internal motional modes provided that they have sufficiently different timescales, and data are collected at multiple fields[25]. Alternatively, data can be analyzed using spectral density mapping approaches that directly map out components of the oscillating magnetic field[26]. The recent determination of the large nucleobase carbon CSAs, which are necessary for interpretation of spin relaxation data, has also addressed a considerable element of uncertainty in data analysis[27–29]. For domain-elongated RNAs, qualitative dynamic information can be obtained by simply comparing the intensity of NMR signals for a given nucleus type in multidimensional spectra[22].

The nuclei that are most commonly targeted for spin-relaxation studies include imino nitrogens in the guanine and uridine nucleobases and protonated carbons in the nucleobases and sugars of all four nucleotides (**Fig. 1**). For ^{13}C relaxation measurements, unwanted ^{13}C-^{13}C interactions are suppressed by using site-specific (**Supplementary Table 1**) or fractional carbon labeling schemes, performing experiments at natural abundance, or by use of appropriate pulse schemes. Pulse sequences that use transverse relaxation–optimized spectroscopy detection schemes can be used to acquire nucleobase ^{13}C relaxation data on large RNAs up to ~150 nucleotides[16].

Common themes are beginning to emerge regarding RNA dynamics at pico- to nanosecond timescales from spin relaxation studies of a wide range of RNA systems[17,30–35]. Watson-Crick as well as noncanonical base pairs tend to experience limited motions ($S^2 > 0.85$) with amplitudes that are comparable to the static variations seen in X-ray structures of A-form helices[36]. Noncanonical residues typically undergo larger, more variable amplitude local motions that tend to be inversely correlated with the extent of stacking[17,30–35]. These motions can occur at timescales comparable to, or slower than, overall tumbling, that is, in the tens to hundreds of nanoseconds timescale[22,37]. Notably, the dynamics of the sugars often, but not always[34], follow the dynamics of the nucleobases, whereas recent ^{31}P relaxation data suggest that the amplitude of backbone motions exceeds that of both the sugar and base moieties[18]. Many of these trends are illustrated in spin-relaxation studies of the structurally well characterized UUCG tetraloop in which limited mobility (S^2 of ~1) is observed for the G·U noncanonical base pair, which stacks on the helix, whereas

much greater mobility (S^2 of 0.68–0.83) is observed for the looped out U7 and partially looped out C8[17,18,32] (**Fig. 2c**). Furthermore, studies show that helices can undergo large amplitude collective motions (S^2 of 0.6–0.8)[16,22,37]. These interhelical motions are, however, not fully captured by spin relaxation because they occur at timescales slower than overall tumbling. Rather, they have been quantitatively characterized with the use of RDCs.

High pico- to nanosecond mobility is often observed in regions that undergo conformational adjustments during catalysis and recognition. For example, analysis of ^{13}C relaxation data using reduced spectral density mapping revealed extensive pico- to nanosecond mobility in key functional groups of the D5 domain from the group II intron that are implicated in binding magnesium ions and catalysis[33] (**Fig. 2d**). A quantitative correlation has been observed between the amplitude of pico- to nanosecond motions at a given site of the HIV-1 transactivation response (TAR) element and the extent to which that site undergoes changes in conformation on binding seven distinct ligands[16,22].

A surprising theme emerging from spin-relaxation studies is that RNA recognition does not necessarily lead to conformational stabilization but, more typically, the reorganization of motional modes, reflecting broader changes across the dynamic structure landscape[33,37,38]. For example, binding of the U1A protein to its cognate RNA target does not lead to the arrest of interhelical motions but induces mobility in regions of the RNA that are in direct contact with the protein[39] (**Fig. 2e**). In contrast, binding of the ligand argininamide to TAR leads to the total arrest of interhelical motions and an increase in the local dynamics of two out of three bulge residues in the interhelical junction[16].

Sub-millisecond motions from residual dipolar couplings

The introduction of partial alignment methods for measuring residual anisotropic interactions, RDCs and RCSAs, which normally average to zero in the solution state[40,41], has extended the timescales of motions that are accessible by NMR spectroscopy beyond those which can be measured by spin relaxation to include all timescales that are faster than ~10 milliseconds. Despite this broader timescale sensitivity, RDCs do not replace spin-relaxation measurements but rather complement them. In particular, RDCs are somewhat less sensitive to the amplitude of motions because they scale with S rather than S^2 and also do not provide information about motional timescales. Thus, RDCs are most effectively used when applied in concert with spin relaxation and also relaxation-dispersion techniques for quantifying micro- to millisecond exchange. Studies using all of these techniques reveal that a given site in RNA can experience multiple motional modes simultaneously, highlighting the complexity of RNA dynamics[33,38,42] (**Fig. 2d**).

To understand how RDCs can be measured via partial alignment, let us consider a C-H bond vector. As mentioned previously, the carbon nucleus experiences the sum of the external magnetic field and the field generated by the proton nucleus. The latter contribution varies as the molecule tumbles: in some orientations the proton field adds to the external magnetic field, whereas in other orientations, it opposes it. This angular dependence is described by

$$\left\langle \frac{3\cos^2\theta - 1}{2} \right\rangle, \qquad (1)$$

in which θ is the angle between the internuclear vector and the magnetic field, and the angular brackets denote a time-average over all orientations sampled at a rate faster than the dipolar coupling (**Fig. 3a**). Under conditions of random Brownian rotational diffusion, the angular term averages to zero, and the proton does not modify the average field at the carbon nucleus, and therefore the observed carbon chemical shift remains unchanged. However, by imparting a small degree of order on the molecule, to the tune of one in 10^3–10^5 molecules being completely aligned, the angular term no longer averages to zero, and the carbon nucleus experiences a residual proton field in addition to the external magnetic field. As half of the proton nuclei are aligned parallel and the other half antiparallel to the field, the proton fields add to the external field for half of the carbon nuclei and subtract for the other half. Consequently, the carbon resonance frequency splits into a doublet, reflecting the addition and subtraction of the average proton field. The magnitude of this splitting is referred to as an RDC[40,41]. A wide range of RDCs involving the base, sugar and backbone moieties can be measured in nucleic acids as reviewed elsewhere[43].

The desired optimum degree of alignment (~10^{-3}) can be achieved by dissolving molecules in magnetically or mechanically ordered media[41,44] that transmit order to the solute by a combination of steric and electrostatic mechanisms. For nucleic acids, the most widely used medium is filamentous bacteriophage (Pf1)[45], which is negatively charged, thus minimizing unwanted

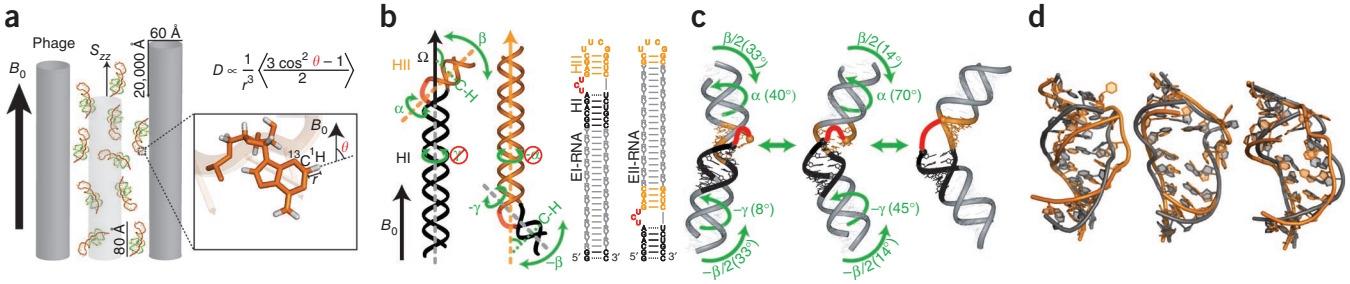

Figure 3 | Characterizing motions over sub-millisecond timescales using residual dipolar couplings. (**a**) Partial alignment of RNA using Pf1 phage shown as gray rods (left) (adapted from ref. 43). (**b**) Domain-elongation for decoupling internal and overall motions allows measurement of bond vector dynamics relative to the elongated helix. An isotopic labeling strategy is used to render elongation residues (R-Y) NMR-invisible (adapted from ref. 52). (**c**) Spatially correlated interhelical motions observed using RDCs involving correlated changes in the interhelical twist (α and γ) and bend (β) angles (adapted from ref. 52). (**d**) Combining domain-elongation RDCs and molecular dynamics simulations in the construction of atomic-resolution dynamic ensembles of TAR reveals conformations (gray) very similar to those observed in ligand bound states (orange) (adapted from ref. 55 with permission from Oxford University Press).

interactions with the nucleic acid, has good tolerance to high ionic strength and is commercially available (**Fig. 3a**). RDCs are typically measured as the difference in splittings observed in the absence and presence of the Pf1 phage medium. Although less commonly used, a smaller (10^{-5}) less ideal degree of alignment can be achieved based on spontaneous alignment of nucleic acids owing to interactions with the magnetic field itself[40,46]. Magnetic field alignment also has a simple dependence on nucleic acid structure, which has been exploited in several unique applications[21,46–48]. By changing the alignment of the solute, up to five independent sets of RDCs can be measured, which can be used to probe motions with greater spatial resolution[49,50]. In proteins, changing alignment can be accomplished by changing the ordering medium[44,51]. This has proven difficult in nucleic acids because their polyanionic nature results in similar steric and electrostatic interactions with different ordering media. Differential domain-elongation and magnetic field alignment offer alterative approaches for modulating the alignment of RNA[48,52].

The angular dependence of RDCs (equation (1)) is time-averaged over both internal and overall motions. Separating and quantifying these two contributions can be difficult in highly flexible systems[43,53]. The interpretation of RDCs is considerably simplified by elongating the RNA so that the overall alignment can be fixed on the elongated helix and used as a reference for measuring averaging contributions owing to internal motions in other parts of the RNA[52] (**Fig. 3b**). Furthermore, by altering which helix is elongated, multiple sets of RDCs can be measured to improve the spatial sensitivity to the dynamics[54] (**Fig. 3b**). Such RDC approaches have revealed collective interhelical motions that are not fully captured by spin-relaxation data. For example, the amplitude of interhelical motions measured in TAR using RDCs (S^2_{RDC} of ~0.20)[52] far exceed those observed by spin relaxation (S^2 of ~0.74)[22], most likely because the interhelical motions include fluctuations at the nano- to microsecond timescale that are inaccessible to spin relaxation[22,42]. Moreover, the measurement of RDCs in two domain-elongated TAR samples (**Fig. 3b**) made it possible to map out its interhelical dynamic trajectory in three dimensions. Results revealed a highly choreographed trajectory in which the two helices bend and twist in a spatially correlated manner[52] (**Fig. 3c**).

By combining domain-elongation RDCs with molecular dynamics simulations, the dynamic ensemble description of RNA was extended to the atomic level[55]. RDCs measured in elongated RNAs were used to guide selection of conformers from a pool generated using molecular dynamics simulations. The ensemble of TAR constructed in this manner was shown to include many conformations that resemble those of TAR observed in various ligand-bound states, providing support for recognition via conformational selection (**Fig. 3d**). More recently, the RDC-derived TAR ensemble was subjected to computational screening to identify anti-HIV therapies that broadly target the TAR dynamic structure landscape[56]. This made it possible to overcome the difficulty in computationally modeling changes in RNA structure that take place upon small molecule binding and led to *de novo* discovery of six small molecules that bind TAR, one of which inhibited HIV replication in T-cell lines *in vivo* with a half-maximal inhibitory concentration of ~20 μM.

Characterizing excited states using relaxation dispersion

Thus far, we have focused on techniques that can be used to study dynamic excursions about the dominant 'ground state' conformation. Much less often, biomolecules transition into different conformational substates, referred to as 'excited states', that populate different local minima along the energy landscape and that require loss of key stabilizing interactions, which are partially restored by formation of new ones (**Fig. 1**). NMR relaxation-dispersion techniques (**Box 2**) allow characterizing the population, lifetime and conformation of these lowly populated (as low as 1%) and transient (lifetimes <1 ms) excited states[57,58].

To understand relaxation dispersion, consider a nucleus that exchanges between a major ground (G) and minor (E) excited state with chemical shifts, ω_G and ω_E, respectively. In the absence of exchange, two NMR peaks are observed with chemical shifts ω_G and ω_E with integrated volumes that reflect their relative populations (**Fig. 4a**). Now consider what happens when G and E states exchange at a rate ($k_{ex} = k_{GE} + k_{EG}$) comparable to their NMR frequency difference ($\Delta\omega = \omega_G - \omega_E$). In this case, the frequency of a given nucleus stochastically fluctuates between ω_G and ω_E. Because nuclei in different molecules spend varying amounts of time in the G and E state, their magnetization no longer precess in synchrony (**Fig. 4b**). The resulting 'fanning out' of the magnetization leads to a decay in the net oscillating signal and an additional exchange contribution (R_{ex}) to transverse relaxation (R_2) (**Fig. 4c**). The broadening of both the excited state and observed peaks is a function of the kinetics and populations of the exchange process. This line broadening can result in the total disappearance of the excited-state signal (**Fig. 4a**). Relaxation dispersion experiments probe the invisible excited state by measuring the exchange broadening contribution to the visible ground-state signal following the application of a series of radiofrequency pulses in the Carr-Purcell-Meiboom-Gill (CPMG) experiment or constant radiofrequency field in the $R_{1\rho}$ experiment, which are designed to suppress the exchange broadening (**Fig. 4b**). For example, in the CPMG experiment, 180° pulses reverse the precession of magnetization at constant time intervals, τ_{cp}; as a result, any dephasing that accrues before the 180° pulse is partly refocused in the following period, with the extent of refocusing increasing with shorter τ_{cp} delays (**Fig. 4b**). The exchange contribution is measured as a function of τ_{cp} in a CPMG experiment and the power and frequency of radiofrequency field in $R_{1\rho}$. The resulting relaxation dispersion curve (**Fig. 4c**) is typically fit to a two-state model. For slow ($k_{ex} << |\Delta\omega|$) to intermediate ($k_{ex} = \sim|\Delta\omega|$) exchange, this yields the population (p_E), lifetime ($\tau_{ex} = 1/k_{ex}$) and chemical shift (ω_E) of the excited state, the latter carrying structural information, whereas for fast exchange ($k_{ex} >> |\Delta\omega|$), only τ_{ex} and $\Phi = p_G p_E \Delta\omega^2$ can be determined and additional experiments are needed to resolve $\Delta\omega$ and p_E. The CPMG experiment only yields the absolute difference in chemical shift $|\omega_E - \omega_G|$, and additional experiments[59,60] are typically needed to determine ω_E.

CPMG relaxation dispersion can be used to probe exchange processes occurring at microsecond to tens of millisecond timescales[57,58]. The CPMG experiment is difficult to apply to nucleic acids because ^{13}C experiments are complicated by extensive ^{13}C-^{13}C scalar couplings that are difficult to suppress owing to challenges in achieving selective carbon excitation with hard 180° pulses[13,61]. This problem has been addressed by preparing RNA samples that are specifically ^{13}C-labeled at the C2′ and C4′ sugar positions[61] (**Fig. 4d**). CPMG experiments on these samples led to the observation of excited-state sugar conformations in the GCAA tetraloop with populations of 15–30% and lifetimes of 30–42 microseconds

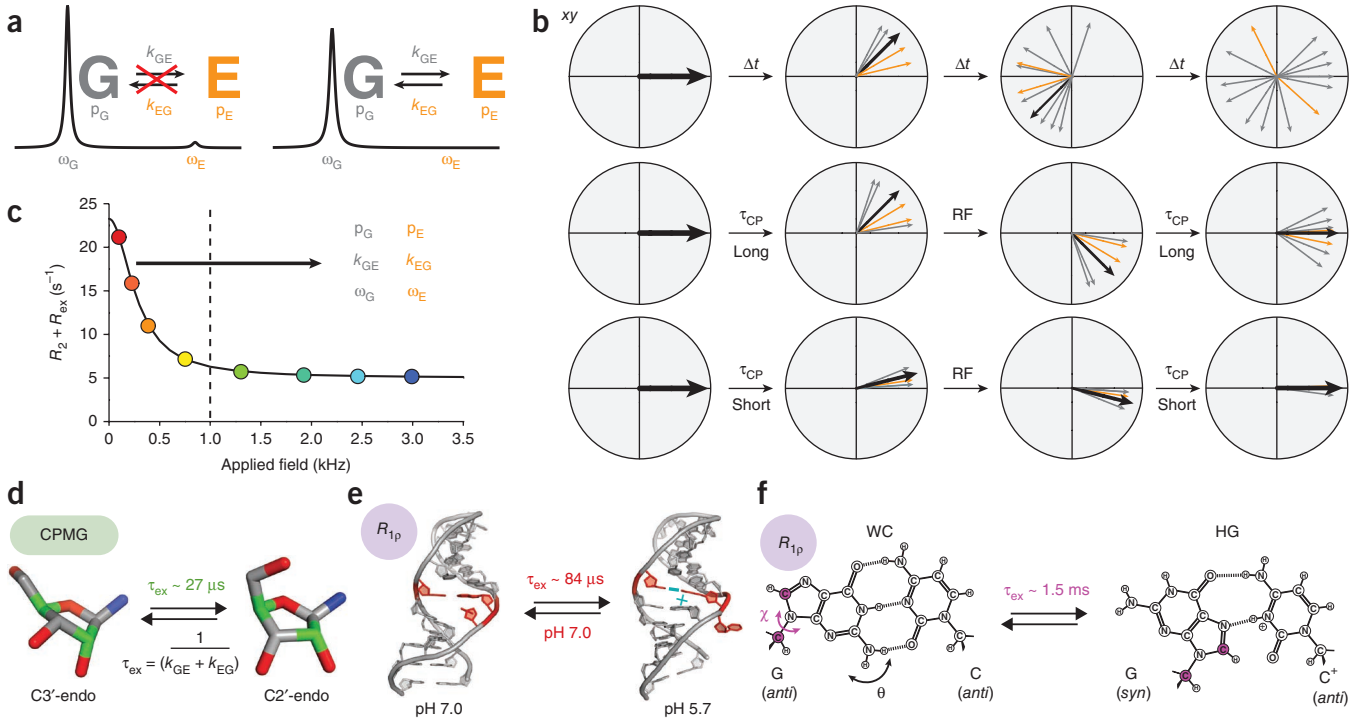

Figure 4 | Characterizing microsecond to millisecond exchange by relaxation dispersion. (**a**) Exchange between ground (G) and excited (E) states leads to broadening of the ground signal and disappearance of the excited signal. (**b**) Fanning out of bulk magnetization due to exchange can be suppressed by application of radiofrequency fields. (**c**) Characteristic relaxation dispersion curve showing the power dependence of R_{ex} which can be used to extract in favorable cases the populations (p), exchange rates (k) and chemical shifts (ω) of ground and excited states. (**d**–**f**) Examples of conformational exchange characterized by a CPMG and $R_{1\rho}$ carbon relaxation dispersion. Sugar repuckering in a GCAA tetraloop using selectively labeled C2′ and C4′ (green) probes[61] (**d**). Transition toward an excited state structure in the U6 RNA involving a C·A$^+$ base pair and looping out of a uridine bulge[68] (**e**). Transition to Hoogsteen (HG) G·C$^+$ base pairs in canonical duplex DNA (**f**; adapted from ref. 70).

that most likely correspond to exchange between C3′-endo and C2′-endo sugar pucker conformations[61] (**Fig. 4d**).

The $R_{1\rho}$ experiment measures line broadening as a function of the power and frequency offset of a constant radiofrequency spin-lock field[62]. The $R_{1\rho}$ experiment has been more widely used than CPMG experiments in studies of nucleic acids because spin lock fields can be used more selectively to reduce or eliminate unwanted ^{13}C-^{13}C interactions. Additional benefits include the ability to directly determine ω_E at a single magnetic field strength without the need for additional experiments[63]. The upper limit for motional timescale is comparable to, if not greater than that of the CPMG experiment (tens to hundreds of microseconds) and is limited by the amount of radiofrequency power that can be dissipated into the probe. Although technical considerations have traditionally limited the lowest radiofrequency spin lock strength to ~1,000 Hz (**Fig. 4c**) and the timescales to exchange processes faster than ~500 microseconds, recent advances permit use of much lower spin lock fields[64–66] (on the order of 100 Hz) extending the timescale sensitivity to tens of milliseconds.

Some of the earliest $R_{1\rho}$ studies revealed microsecond timescale exchange processes involving an excited state C·A$^+$ protonated base pair in the active site of the lead-dependent ribozyme that may be important for catalysis[67]. More recent studies suggest that excited states that are coupled to protonation of nucleobases may be quite common. For example, a microsecond timescale exchange processes directed toward an excited state structure was found, involving a C·A$^+$ base pair in a functionally important region of the U6 RNA element from the spliceosome, which is accompanied by the looping out of a uridine bulge[68,69] (**Fig. 4e**), whereas an even slower millisecond exchange process was found, directed toward excited state G·C$^+$ Hoogsteen base pairs in canonical duplex DNA[70] (**Fig. 4f**). These studies are rare examples in which the structure of the excited state could be determined. This was accomplished by trapping the excited state, either by lowering the pH or by introducing chemical modifications. With these structures in hand, the authors gained insights into the conformational pathway linking the ground and excited states using various computational methods[70,71], highlighting another important area of synergy between NMR spectroscopy and computation.

Slow, greater than millisecond motions from ZZ-exchange and time-resolved NMR spectroscopy

Many RNA dynamic transitions involve changes in secondary structure, which in turn require disruption of several base pairs and can occur at timescales slower than milliseconds. Such transitions can yield separate well-resolved NMR signals for the exchanging species, and in such cases, can be studied using a combination of ZZ-exchange and time-resolved NMR spectroscopy (**Box 2**).

ZZ-exchange spectroscopy can be used to characterize transitions occurring between ~10-millisecond and 1-second timescales. The exchanging species must have well-resolved and detectable NMR signals and must therefore typically be >30% populated. The transition has to be slow enough to avoid extensive exchange broadening but fast enough to allow multiple exchange

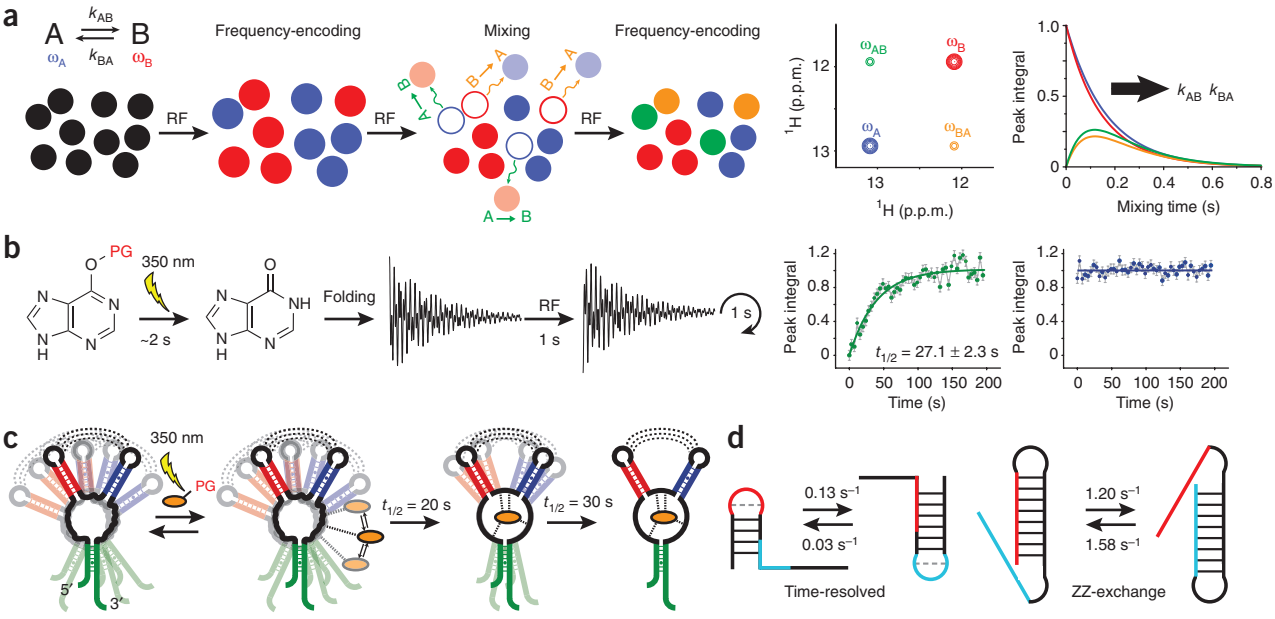

Figure 5 | Characterizing conformational transitions occurring at millisecond and longer timescales by ZZ-exchange and time-resolved NMR spectroscopy. (**a**,**b**) Schematic of (**a**) ZZ-exchange and (**b**) time-resolved NMR spectroscopy experiment. (**c**) Visualizing a multistep ligand-induced conformational transition in the guanine sensing riboswitch using laser induced time-resolved NMR spectroscopy (adapted from ref. 76 with permission from the National Academy of Sciences, USA). (**d**) Characterizing slow and fast RNA refolding rates by time-resolved and ZZ-exchange NMR spectroscopy, respectively.

events to take place while magnetization is stored along the *z* axis during the ZZ-exchange experiment (that is, exchange has to be fast compared to longitudinal relaxation, R_1). Here, an initial frequency-encoding period is used to label the exchanging species, A and B, with their NMR frequencies, ω_A and ω_B (**Fig. 5a**). This is followed by a variable 'mixing period' during which magnetization is stored along the *z* axis (parallel to the magnetic field) and species allowed to exchange. This is followed by a second frequency-encoding period. A two-dimensional (2D) spectrum is constructed correlating the frequencies observed in the two periods (**Fig. 5a**). Molecules that do not exchange during the mixing period or that exchange multiple times back to the original state appear as diagonal cross-peaks with frequencies ω_A/ω_A and ω_B/ω_B, whereas molecules that exchange to a different A or B state appear as off-diagonal cross peaks with frequencies ω_A/ω_B and ω_B/ω_A. The peak intensities of all cross peaks are measured as a function of the mixing period (**Fig. 5a**) and are fit to appropriate equations to obtain the forward and reverse rate constants (k_1 and k_{-1}) for the A to B interconversion. The experiment is optimally carried out using nuclei with long R_1 relaxation times, typically imino protons or as demonstrated more recently using imino nitrogens, which have approximately tenfold slower R_1 relaxation, thus extending sensitivity to slower processes[72]. Alternatively, ^{13}C-labeled methyl groups, which have high sensitivity, spectral resolution and minimal ^{13}C-^{13}C interactions can be introduced onto the 2′ OH groups of uridines and used in ^{13}C ZZ-exchange experiments for studying transitions in large RNAs[19].

Time-resolved NMR experiments can be used to monitor transitions from a non-equilibrium to equilibrium state by repeatedly acquiring 1D or 2D NMR spectra with repetition rates that are on the order of ~2 seconds. This permits characterization of processes occurring at second and slower timescales[73]. Simple mixing of the RNA with suitable reagents can be used to monitor transitions occurring at slower than 1-min timescales. Faster processes (<1 min) require laser excitation or rapid mixing, which reduce dead times to ~1 s (refs. 73,74). In the former, a bulky photolabile group (**Fig. 5b**) is used to protect a ligand or bias an RNA structure toward one of many competing conformations. One typically follows the appearance and disappearance of imino proton signals because they provide high spectral resolution and directly report on formation and loss of base pairs and therefore RNA secondary structure (**Fig. 5b**). Site-specific isotopic labeling schemes or the acquisition of multidimensional spectra using new ultrafast methods can help alleviate spectral congestion, which becomes increasingly important for larger RNAs[74].

ZZ-exchange and time-resolved NMR spectroscopy have allowed the characterization of ligand-induced structural transitions occurring over a wide range of timescales and involving distinct mechanisms. For example, ^{1}H ZZ-exchange revealed that the theophylline RNA aptamer exchanges between its free and structurally more ordered ligand-bound form at second timescales[75]. By contrast, time-resolved NMR spectroscopy allowed the kinetic and site-specific resolution of two distinct kinetic steps occurring on the order of tens of seconds during the ligand induced structural transition of a 73-nucleotide guanine-sensing riboswitch[76] (**Fig. 5c**). The two steps follow rapid formation of an encounter complex and likely involve insertion of the ligand into the binding pocket within the three-way junction followed by formation of tertiary loop-loop interactions that stabilize the ligand-bound structure (**Fig. 5c**).

ZZ-exchange and time-resolved NMR spectroscopy have also allowed the characterization of RNA-refolding transitions occurring over a wide range of timescales and involving distinct mechanisms. These studies have targeted model bistable RNAs, which fold into two distinct but nearly energetically equivalent secondary structures. For example, time-resolved NMR spectroscopy experiments revealed that a bistable 20-nucleotide RNA[77] refolds at second timescales, whereas ^{15}N imino nitrogen ZZ-exchange

experiments revealed even faster refolding rates at hundreds of milliseconds for a large 34-nucleotide sequence (**Fig. 5d**)[72]. Together, these studies suggest that the rate of RNA secondary structural transitions is governed both by the number of bases that have to be disrupted during the transition[77–79] and also the RNA topology[72,73] and relative spatial placement of strands that have to exchange. Additional insights into refolding mechanisms have been obtained from combining these experiments with hydrogen and hydrogen-deuterium exchange experiments described below.

Base-pair-opening dynamics

Many genetic RNA switches, including those that involve change in secondary structure outlined above, require the melting or annealing of strands. At the microscopic level, the underlying dynamics involve the opening of individual base pairs. Characterizing base-pair-opening dynamics is extremely challenging given that the open state typically has miniscule populations that are on the order of 10^{-3} to 10^{-7}% with exceptionally short lifetimes on the order of nanoseconds. NMR spectroscopy experiments probing hydrogen exchange (H exchange) and hydrogen-deuterium exchange (H-D exchange) allow the characterization of base-pair-opening dynamics with site-specific resolution[80,81]. H and H-D exchange measurements have a long history of probing nucleic-acid stability, providing some of the earliest NMR dynamics measurements of DNA and RNA. The experiments take advantage of the fact that when individual base pairs open, imino or amino protons can exchange with solvent[82], resulting in a perturbation of the observed NMR signal (**Fig. 6a**). Analogous to ZZ-exchange and time-resolved NMR methods, two experimental schemes are used to probe exchange at different timescales[80,81]. Exchange times slower than ~10^2–10^3 seconds can be measured by rapidly immersing a protonated RNA sample into D_2O buffer and monitoring the disappearance of imino proton signals over time using 1D or 2D NMR spectroscopy (similar to time-resolved experiments). Faster exchange rates ranging from ~10 seconds to 5 milliseconds can be measured by selectively perturbing the magnetization of water protons and following how this perturbation is transmitted to exchangeable RNA protons during a variable mixing period (similar to ZZ-exchange experiments). Data are typically collected as a function of base catalyst concentration to extract individual opening and closing rate constants and the base-pair-opening equilibrium constant ($K_{op} = \tau_{cl}/\tau_{op}$) permitting determination of the opening and activation free energies.

H and H-D exchange experiments reveal that base-pair lifetimes can range from <1 millisecond to many days, with short (1–50 ms) lifetimes typically observed for A-form helical A·U, G·C and G·U base pairs[83,84], intermediate lifetimes of several seconds for poly(G)-poly(C)[85], up to minutes for base pairs and triplets part of tertiary folds[86] and lifetimes on the order of days for hydrogen-bonding interactions involved in DNA and RNA quadruplexes[87,88] and stable tertiary networks[89]. Lifetimes for the open base pair state are ~1–200 nanoseconds for internal duplex residues[83], with longer lifetimes up to 1–2 microseconds observed for base pairs at the 5′ end of AU tracts[84] or near loops and bulges, which are often believed to be sites for triggering secondary structural rearrangements.

The measured base-pair-opening equilibrium constants typically span a large range between 10^{-9} to 10^{-5} for Watson-Crick base pairs[83,84,90,91] and surprisingly stable G·G mismatch base pairs[90] and up to ~10^{-3} for less stable A·U and G·U base pairs[91], G·A mismatches[92] and bulged or *syn* G imino protons stabilized by contacts with backbone or tertiary H-bond acceptors[90]. The corresponding opening free energies are ~3–10 kcal mol^{-1}. Base-pair opening is accompanied by a large increase in both enthalpy and entropy, up to about tenfold larger than the change in free energy, signifying loss of favorable interaction energy with neighboring nucleotides and gain of favorable entropy arising in part from conformational flexibility in the open state.

H-exchange experiments, when combined with time-resolved and ZZ-exchange experiments, provide insights into the refolding mechanism of bistable RNAs. Dissociative refolding mechanisms involve partial unfolding of the RNA followed by formation of stabilizing contacts that lead to a competing secondary structure, whereas associative mechanisms involve an intermediate in which structural elements join to form contacts of the competing secondary structure followed by dissociation of existing stabilizing contacts. The refolding mechanisms of two 20-nucleotide RNAs[77,78] were deduced by comparing imino proton exchange rates measured for sequences able and unable to refold. Similar imino proton exchange rate patterns are indicative of dissociative mechanisms, whereas enhanced exchange rates near the site of association in the RNA suggest an associative mechanism. The authors found that the mechanism type is encoded by the particular topology of refolding RNA sequences[73].

Another example using H-exchange experiments is the temperature labile *Salmonella enterica* FourU RNA thermometer, which regulates gene expression at the translational level by undergoing a melting transition in response to changes in temperature[91] (**Fig. 6b**). An inactive single-point mutant was used to deconstruct differences in macroscopic RNA unfolding in terms of microscopic unfolding events (**Fig. 6b**). The authors observed strong enthalpy-entropy compensation, which argues that global unfolding occurs when microscopic base-pair stabilities are equalized. A single G·A to G·C Watson-Crick mutation was observed to

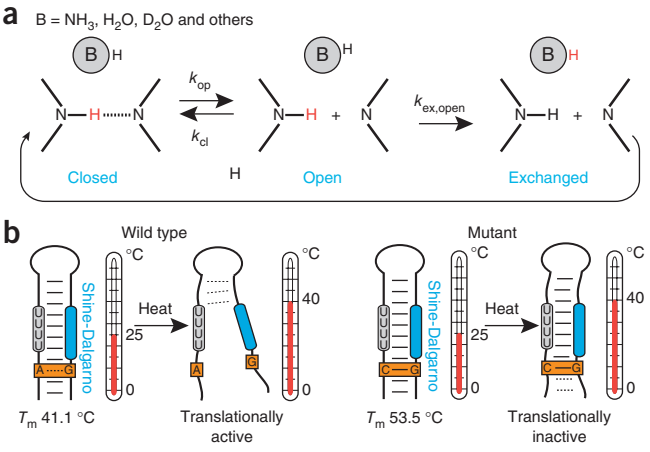

Figure 6 | Characterizing base-pair-opening dynamics by imino proton exchange. (**a**) Schematic of a two-step (direct or water-mediated) imino proton exchange for an RNA base pair catalyzed by a proton acceptor B, followed by reversible base-pair formation. H exchange experiments can be used to measure rate constants in each step. (**b**) Imino proton exchange study of the wild-type (left) *Salmonella* FourU RNA thermometer and its translationally inactive GA-to-GC mutant (right), showed a correlation between changes in local base-pair stabilities and changes in global melting profiles of the wild-type and mutant constructs[91].

stabilize base pairs close and far-removed from the site of mutation, possibly via an extended hydration network, which globally translates into an enhanced overall hairpin thermostability and folding cooperativity providing an explanation for its lack of *in vivo* activity at physiological temperatures.

Summary and future perspective

Thanks to many developments in solution-state NMR methodology over the past decade, new aspects of the RNA dynamic structure landscape are beginning to emerge, at least in outline. In **Box 2**, we outline avenues for specific future technical developments in NMR methods for dynamics measurements. We also identify three general challenges for the future. First, the accessible experimental data are not sufficient to comprehensively and unambiguously characterize the RNA dynamic structure landscape at atomic resolution. To overcome this challenge, other sources of NMR information have to be tapped, including chemical shifts[93,94], paramagnetic relaxation enhancement[95], RDC or RCSA relaxation dispersion experiments[96] and also, powerful information that can be obtained from solid-state NMR methods[97]. Solution-state NMR methods are also hindered by size limitations due to spectral overcrowding of resonances and enhanced line broadening with increasing molecular weight. Therefore, data from other techniques including small-angle X-ray scattering[98] and chemical footprinting[99] will also be important for enabling studies of much larger RNAs. Most importantly, input from computational methods will be critical, and there is an urgent need to continue to test and develop nucleic acid force fields using NMR spectroscopy[32,55]. Second, there is a need to better understand how the RNA dynamic structure landscape depends on sequence, secondary and tertiary structure, and metals. To meet this goal, the dynamic properties of RNA structure have to be more systematically pursued using a range of strategically well-chosen RNA systems and conditions. Last but not least, this dynamic description of RNA has to be translated into a better more predictive understanding of function. The link between RNA dynamics and function remains vague and qualitative. Regions that change during functional cycles tend to be flexible; in few cases, aspects of sequence and secondary structure seem to have evolutionally conserved dynamic roles. To make this relationship more quantitative, kinetic, thermodynamic and structural properties of RNA dynamics have to be surgically perturbed with the use of mutagenesis, chemical modifications or external agents, and the consequences on functional readouts firmly established. Likewise, there is a need to better characterize and understand how cellular cues broadly affect the RNA dynamic structure landscape.

The current rejuvenated interest in solution-state NMR spectroscopy of RNA will very likely lead to unanticipated advances and discoveries regarding the basic physical behavior of RNA. We hope that this review will help spark interest in pursuing many of these future applications.

Note: Supplementary information is available on the Nature Methods website.

ACKNOWLEDGMENTS

We thank members of the Al-Hashimi lab for insightful comments and A. Kurochkin for maintenance of the NMR instruments. We acknowledge collaborations with the groups of C. Fierke (University of Michigan), I. Andricioaei (University of California, Irvine) and C. Brooks (University of Michigan), and the Michigan Economic Development Cooperation and the Michigan Technology Tri-Corridor for the support of the purchase of a 600-MHz spectrometer. This work was supported by the US National Institutes of Health (R01 AI066975 and R01 GM089846) and the US National Science Foundation Career Award (MCB 0644278).

COMPETING FINANCIAL INTERESTS

The authors declare competing financial interests: details accompany the full-text HTML version of the paper at http://www.nature.com/naturemethods/.

Published online at http://www.nature.com/naturemethods/.
Reprints and permissions information is available online at http://www.nature.com/reprints/index.html.

1. Frauenfelder, H., Sligar, S.G. & Wolynes, P.G. The energy landscapes and motions of proteins. *Science* **254**, 1598–1603 (1991).
2. Cruz, J.A. & Westhof, E. The dynamic landscapes of RNA architecture. *Cell* **136**, 604–609 (2009).
3. Blount, K.F. & Breaker, R.R. Riboswitches as antibacterial drug targets. *Nat. Biotechnol.* **24**, 1558–1564 (2006).
4. Micura, R. & Hobartner, C. On secondary structure rearrangements and equilibria of small RNAs. *ChemBioChem* **4**, 984–990 (2003).
5. Cooper, T.A., Wan, L.L. & Dreyfuss, G. RNA and disease. *Cell* **136**, 777–793 (2009).
6. Hermann, T. Rational ligand design for RNA: the role of static structure and conformational flexibility in target recognition. *Biochimie* **84**, 869–875 (2002).
7. Banas, P. *et al.* Performance of molecular mechanics force fields for RNA simulations: stability of UUCG and GNRA hairpins. *J. Chem. Theory Comput.* **6**, 3836–3849 (2010).
8. Boehr, D.D., Nussinov, R. & Wright, P.E. The role of dynamic conformational ensembles in biomolecular recognition. *Nat. Chem. Biol.* **5**, 789–796 (2009).
9. Leulliot, N. & Varani, G. Current topics in RNA-protein recognition: control of specificity and biological function through induced fit and conformational capture. *Biochemistry* **40**, 7947–7956 (2001).
10. Al-Hashimi, H.M. & Walter, N.G. RNA dynamics: it is about time. *Curr. Opin. Struct. Biol.* **18**, 321–329 (2008).
11. Palmer, A.G. NMR characterization of the dynamics of biomacromolecules. *Chem. Rev.* **104**, 3623–3640 (2004).
12. Furtig, B., Richter, C., Wohnert, J. & Schwalbe, H. NMR spectroscopy of RNA. *ChemBioChem* **4**, 936–962 (2003).
13. Yamazaki, T., Muhandiram, R. & Kay, L.E. NMR experiments for the measurement of carbon relaxation properties in highly enriched, uniformly C-13,N-15-labeled proteins—application to C-13(alpha) carbons. *J. Am. Chem. Soc.* **116**, 8266–8278 (1994).
14. Boisbouvier, J., Wu, Z., Ono, A., Kainosho, M. & Bax, A. Rotational diffusion tensor of nucleic acids from ^{13}C NMR relaxation. *J. Biomol. NMR* **27**, 133–142 (2003).
15. Johnson, J.E. Jr., Julien, K.R. & Hoogstraten, C.G. Alternate-site isotopic labeling of ribonucleotides for NMR studies of ribose conformational dynamics in RNA. *J. Biomol. NMR* **35**, 261–274 (2006).
16. Hansen, A.L. & Al-Hashimi, H.M. Dynamics of large elongated RNA by NMR carbon relaxation. *J. Am. Chem. Soc.* **129**, 16072–16082 (2007).
17. Vallurupalli, P. & Kay, L.E. A suite of 2H NMR spin relaxation experiments for the measurement of RNA dynamics. *J. Am. Chem. Soc.* **127**, 6893–6901 (2005).
18. Rinnenthal, J. *et al.* RNA phosphodiester backbone dynamics of a perdeuterated cUUCGg tetraloop RNA from phosphorus-31 NMR relaxation analysis. *J. Biomol. NMR* **45**, 143–155 (2009).
19. Kloiber, K., Spitzer, R., Tollinger, M., Konrat, R. & Kreutz, C. Probing RNA dynamics via longitudinal exchange and CPMG relaxation dispersion NMR spectroscopy using a sensitive 13C-methyl label. *Nucleic Acids Res.* **39**, 4340–4351 (2011).
20. Lipari, G. & Szabo, A. Model-free approach to the interpretation of nuclear magnetic-resonance relaxation in macromolecules. 1. Theory and range of validity. *J. Am. Chem. Soc.* **104**, 4546–4559 (1982).
21. Zhang, Q., Throolin, R., Pitt, S.W., Serganov, A. & Al-Hashimi, H.M. Probing motions between equivalent RNA domains using magnetic field induced residual dipolar couplings: Accounting for correlations between motions and alignment. *J. Am. Chem. Soc.* **125**, 10530–10531 (2003).
22. Zhang, Q., Sun, X., Watt, E.D. & Al-Hashimi, H.M. Resolving the motional modes that code for RNA adaptation. *Science* **311**, 653–656 (2006).

23. Showalter, S.A., Baker, N.A., Tang, C.G. & Hall, K. Iron responsive element RNA flexibility described by NMR and isotropic reorientational eigenmode dynamics. *J. Biomol. NMR* **32**, 179–193 (2005).
24. Showalter, S.A. & Hall, K.B. Correlated motions in the U1 snRNA stem/loop 2: U1A RBD1 complex. *Biophys. J.* **89**, 2046–2058 (2005).
25. Clore, G.M. *et al.* Deviations from the simple 2-parameter model-free approach to the interpretation of N-15 nuclear magnetic-relaxation of proteins. *J. Am. Chem. Soc.* **112**, 4989–4991 (1990).
26. Peng, J.W. & Wagner, G. Mapping of the spectral densities of N-H bond motions in eglin c using heteronuclear relaxation experiments. *Biochemistry* **31**, 8571–8586 (1992).
27. Stueber, D. & Grant, D.M. ^{13}C and ^{15}N chemical shift tensors in adenosine, guanosine dihydrate, 2′-deoxythymidine, and cytidine. *J. Am. Chem. Soc.* **124**, 10539–10551 (2002).
28. Hansen, A.L. & Al-Hashimi, H.M. Insight into the CSA tensors of nucleobase carbons in RNA polynucleotides from solution measurements of residual CSA: towards new long-range orientational constraints. *J. Magn. Reson.* **179**, 299–307 (2006).
29. Ying, J.F., Grishaev, A., Bryce, D.L. & Bax, A. Chemical shift tensors of protonated base carbons in helical RNA and DNA from NMR relaxation and liquid crystal measurements. *J. Am. Chem. Soc.* **128**, 11443–11454 (2006).
This study reports the determination of the nucleobase carbon CSA tensors in helical RNA and DNA, which are necessary for properly interpreting carbon spin relaxation data in terms of fast picosecond-to-nanosecond dynamics.
30. Akke, M., Fiala, R., Jiang, F., Patel, D. & Palmer, A.G., III. Base dynamics in a UUCG tetraloop RNA hairpin characterized by ^{15}N spin relaxation: correlations with structure and stability. *RNA* **3**, 702–709 (1997).
31. Duchardt, E. & Schwalbe, H. Residue specific ribose and nucleobase dynamics of the cUUCGg RNA tetraloop motif by MNMR ^{13}C relaxation. *J. Biomol. NMR* **32**, 295–308 (2005).
32. Ferner, J. *et al.* NMR and MD studies of the temperature-dependent dynamics of RNA YNMG-tetraloops. *Nucleic Acids Res.* **36**, 1928–1940 (2008).
33. Eldho, N.V. & Dayie, K.T. Internal bulge and tetraloop of the catalytic domain 5 of a group II intron ribozyme are flexible: implications for catalysis. *J. Mol. Biol.* **365**, 930–944 (2007).
Highlighting the complexity of the RNA structure dynamic landscape, the authors report motions occuring at fast (picosecond to nanosecond) and slow (microsecond to millisecond) timescales that are modulated by the presence of Mg^{2+} ions.
34. Oberstrass, F.C., Allain, F.H. & Ravindranathan, S. Changes in dynamics of SRE-RNA on binding to the VTS1p-SAM domain studied by ^{13}C NMR relaxation. *J. Am. Chem. Soc.* **130**, 12007–12020 (2008).
35. Ampt, K.A.M., van der Werf, R.M., Nelissen, F.H.T., Tessari, M. & Wijmenga, S.S. The unstable part of the apical stem of duck hepatitis B virus epsilon shows enhanced base pair opening but not pico- to nanosecond dynamics and is essential for reverse transcriptase binding. *Biochemistry* **48**, 10499–10508 (2009).
36. Musselman, C. *et al.* Impact of static and dynamic A-form heterogeneity on the determination of RNA global structural dynamics using NMR residual dipolar couplings. *J. Biomol. NMR* **36**, 235–249 (2006).
37. Sun, X., Zhang, Q. & Al-Hashimi, H.M. Resolving fast and slow motions in the internal loop containing stem-loop 1 of HIV-1 that are modulated by Mg^{2+} binding: role in the kissing-duplex structural transition. *Nucleic Acids Res.* **35**, 1698–1713 (2007).
38. Bardaro, M.F., Shajani, Z., Patora-Komisarska, K., Robinson, J.A. & Varani, G. How binding of small molecule and peptide ligands to HIV-1 TAR alters the RNA motional landscape. *Nucleic Acids Res.* **37**, 1529–1540 (2009).
39. Shajani, Z., Drobny, G. & Varani, G. Binding of U1A protein changes RNA dynamics as observed by ^{13}C NMR relaxation studies. *Biochemistry* **46**, 5875–5883 (2007).
This study highlights the complex manner in which protein binding transforms the RNA dynamic structure landscape; interhelical motions are minimally perturbed while residues that directly interact with the protein are either rigidified or become more flexible.
40. Tolman, J.R., Flanagan, J.M., Kennedy, M.A. & Prestegard, J.H. Nuclear magnetic dipole interactions in field-oriented proteins—information for structure determination in solution. *Proc. Natl. Acad. Sci. USA* **92**, 9279–9283 (1995).
41. Tjandra, N. & Bax, A. Direct measurement of distances and angles in biomolecules by NMR in a dilute liquid crystalline medium. *Science* **278**, 1111–1114 (1997).
42. Dethoff, E.A. *et al.* Characterizing complex dynamics in the transactivation response element apical loop and motional correlations with the bulge by NMR, molecular dynamics, and mutagenesis. *Biophys. J.* **95**, 3906–3915 (2008).
43. Getz, M., Sun, X., Casiano-Negroni, A., Zhang, Q. & Al-Hashimi, H.M. NMR studies of RNA dynamics and structural plasticity using NMR residual dipolar couplings. *Biopolymers* **86**, 384–402 (2007).
44. Tolman, J.R. & Ruan, K. NMR residual dipolar couplings as probes of biomolecular dynamics. *Chem. Rev.* **106**, 1720–1736 (2006).
45. Hansen, M.R., Mueller, L. & Pardi, A. Tunable alignment of macromolecules by filamentous phage yields dipolar coupling interactions. *Nat. Struct. Biol.* **5**, 1065–1074 (1998).
46. Kung, H.C., Wang, K.Y., Goljer, I. & Bolton, P.H. Magnetic alignment of duplex and quadruplex DNAs. *J. Magn. Reson. B.* **109**, 323–325 (1995).
47. Tjandra, N., Omichinski, J.G., Gronenborn, A.M., Clore, G.M. & Bax, A. Use of dipolar H-1-N-15 and H-1-C-13 couplings in the structure determination of magnetically oriented macromolecules in solution. *Nat. Struct. Biol.* **4**, 732–738 (1997).
48. Zhang, Q. & Al-Hashimi, H.M. Extending the NMR spatial resolution limit for RNA by motional couplings. *Nat. Methods* **5**, 243–245 (2008).
49. Peti, W., Meiler, J., Bruschweiler, R. & Griesinger, C. Model-free analysis of protein backbone motion from residual dipolar couplings. *J. Am. Chem. Soc.* **124**, 5822–5833 (2002).
50. Fisher, C.K. & Al-Hashimi, H.M. Approximate reconstruction of continuous spatially complex domain motions by multialignment NMR residual dipolar couplings. *J. Phys. Chem. B* **113**, 6173–6176 (2009).
51. Ramirez, B.E. & Bax, A. Modulation of the alignment tensor of macromolecules dissolved in a dilute liquid crystalline medium. *J. Am. Chem. Soc.* **120**, 9106–9107 (1998).
52. Zhang, Q., Stelzer, A.C., Fisher, C.K. & Al-Hashimi, H.M. Visualizing spatially correlated dynamics that directs RNA conformational transitions. *Nature* **450**, 1263–1267 (2007).
This study combined domain elongation and RDCs to construct a 3D trajectory of the interhelical motions in TAR RNA; the interhelical trajectory shows that TAR can dynamically sample seven distinct ligand-bound states in the absence of ligands.
53. Tolman, J.R. & Ruan, K. NMR residual dipolar couplings as probes of biomolecular dynamics. *Chem. Rev.* **106**, 1720–1736 (2006).
54. Fisher, C.K., Zhang, Q., Stelzer, A. & Al-Hashimi, H.M. Ultrahigh resolution characterization of domain motions and correlations by multialignment and multireference residual dipolar coupling NMR. *J. Phys. Chem. B* **112**, 16815–16822 (2008).
55. Frank, A.T., Stelzer, A.C., Al-Hashimi, H.M. & Andricioaei, I. Constructing RNA dynamical ensembles by combining MD and motionally decoupled NMR RDCs: new insights into RNA dynamics and adaptive ligand recognition. *Nucleic Acids Res.* **37**, 3670–3679 (2009).
56. Stelzer, A.C. *et al.* Discovery of selective bioactive small molecules by targeting an RNA dynamic ensemble. *Nat. Chem. Biol.* **7**, 553–559 (2011).
57. Palmer, A.G., Kroenke, C.D. & Loria, J.P. Nuclear magnetic resonance methods for quantifying microsecond-to-millisecond motions in biological macromolecules. *Methods Enzymol.* **339**, 204–238 (2001).
58. Korzhnev, D.M. & Kay, L.E. Probing invisible, low-populated states of protein molecules by relaxation dispersion NMR spectroscopy: an application to protein folding. *Acc. Chem. Res.* **41**, 442–451 (2008).
59. Skrynnikov, N.R., Dahlquist, F.W. & Kay, L.E. Reconstructing NMR spectra of "invisible" excited protein states using HSQC and HMQC experiments. *J. Am. Chem. Soc.* **124**, 12352–12360 (2002).
60. Auer, R. *et al.* Measurement of signs of chemical shift differences between ground and excited protein states: a comparison between H(S/M)QC and R-1 rho methods. *J. Biomol. NMR* **46**, 205–216 (2010).
61. Johnson, J.E. Jr. & Hoogstraten, C.G. Extensive backbone dynamics in the GCAA RNA tetraloop analyzed using ^{13}C NMR spin relaxation and specific isotope labeling. *J. Am. Chem. Soc.* **130**, 16757–16769 (2008).
Site-specific carbon labeling makes it possible to apply carbon CPMG relaxation dispersion experiments and lead to the observation of conformational exchange within the sugars of an apical loop.
62. Palmer, A.G. & Massi, F. Characterization of the dynamics of biomacromolecules using rotating-frame spin relaxation NMR spectroscopy. *Chem. Rev.* **106**, 1700–1719 (2006).
63. Trott, O. & Palmer, A.G. R-1 rho relaxation outside of the fast-exchange limit. *J. Magn. Reson.* **154**, 157–160 (2002).
64. Massi, F., Johnson, E., Wang, C.Y., Rance, M. & Palmer, A.G. NMR R-1 rho rotating-frame relaxation with weak radio frequency fields. *J. Am. Chem. Soc.* **126**, 2247–2256 (2004).

65. Korzhnev, D.M., Orekhov, V.Y. & Kay, L.E. Off-resonance R1(p) NMR studies of exchange dynamics in proteins with low spin-lock fields: An application to a fyn SH3 domain. *J. Am. Chem. Soc.* **127**, 713–721 (2005).
66. Hansen, A.L., Nikolova, E.N., Casiano-Negroni, A. & Al-Hashimi, H.M. Extending the range of microsecond-to-millisecond chemical exchange detected in labeled and unlabeled nucleic acids by selective carbon R(1rho) NMR spectroscopy. *J. Am. Chem. Soc.* **131**, 3818–3819 (2009).
This paper describes application of low-spin lock power $R_{1\rho}$ experiments for characterizing slow millisecond exchange processes in DNA and RNA.
67. Hoogstraten, C.G., Wank, J.R. & Pardi, A. Active site dynamics in the lead-dependent ribozyme. *Biochemistry* **39**, 9951–9958 (2000).
68. Blad, H., Reiter, N.J., Abildgaard, F., Markley, J.L. & Butcher, S.E. Dynamics and metal ion binding in the U6 RNA intramolecular stem-loop as analyzed by NMR. *J. Mol. Biol.* **353**, 540–555 (2005).
This study combines NMR relaxation dispersion measurements with complementary structural data to propose an RNA excited state.
69. Reiter, N.J., Blad, H., Abildgaard, F. & Butcher, S.E. Dynamics in the U6 RNA intramolecular stem-loop: a base flipping conformational change. *Biochemistry* **43**, 13739–13747 (2004).
70. Nikolova, E.N. *et al.* Transient Hoogsteen base pairs in canonical duplex DNA. *Nature* **470**, 498–502 (2011).
71. Venditti, V., Clos, L., Niccolai, N. & Butcher, S.E. Minimum-energy path for a U6 RNA conformational change involving protonation, base-pair rearrangement and base flipping. *J. Mol. Biol.* **391**, 894–905 (2009).
72. Wenter, P., Bodenhausen, G., Dittmer, J. & Pitsch, S. Kinetics of RNA refolding in dynamic equilibrium by ^{1}H-detected ^{15}N exchange NMR spectroscopy. *J. Am. Chem. Soc.* **128**, 7579–7587 (2006).
73. Furtig, B. *et al.* Time-resolved NMR studies of RNA folding. *Biopolymers* **86**, 360–383 (2007).
74. Lee, M.K., Gal, M., Frydman, L. & Varani, G. Real-time multidimensional NMR follows RNA folding with second resolution. *Proc. Natl. Acad. Sci. USA* **107**, 9192–9197 (2010).
75. Latham, M.P., Zimmermann, G.R. & Pardi, A. NMR chemical exchange as a probe for ligand-binding kinetics in a theophylline-binding RNA aptamer. *J. Am. Chem. Soc.* **131**, 5052–5053 (2009).
76. Buck, J., Furtig, B., Noeske, J., Wohnert, J. & Schwalbe, H. Time-resolved NMR methods resolving ligand-induced RNA folding at atomic resolution. *Proc. Natl. Acad. Sci. USA* **104**, 15699–15704 (2007).
Time-resolved NMR spectroscopy is used to monitor conformational changes in an aptamer domain of an RNA riboswitch that are triggered following ligand binding.
77. Wenter, P., Furtig, B., Hainard, A., Schwalbe, H. & Pitsch, S. Kinetics of photoinduced RNA refolding by real-time NMR spectroscopy. *Angew. Chem. Int. Edn.* **44**, 2600–2603 (2005).
78. Wenter, P., Furtig, B., Hainard, A., Schwalbe, H. & Pitsch, S. A caged uridine for the selective preparation of an RNA fold and determination of its refolding kinetics by real-time NMR. *ChemBioChem* **7**, 417–420 (2006).
79. Furtig, B. *et al.* Conformational dynamics of bistable RNAs studied by time-resolved NMR spectroscopy. *J. Am. Chem. Soc.* **129**, 16222–16229 (2007).
80. Gueron, M. & Leroy, J.L. Studies of base pair kinetics by NMR measurement of proton exchange. *Methods Enzymol.* **261**, 383–413 (1995).
81. Russu, I.M. Probing site-specific energetics in proteins and nucleic acids by hydrogen exchange and nuclear magnetic resonance spectroscopy. *Methods Enzymol.* **379**, 152–175 (2004).
82. Gueron, M., Kochoyan, M. & Leroy, J.L. A single mode of DNA base-pair opening drives imino proton exchange. *Nature* **328**, 89–92 (1987).
83. Snoussi, K. & Leroy, J.L. Imino proton exchange and base-pair kinetics in RNA duplexes. *Biochemistry* **40**, 8898–8904 (2001).
84. Huang, Y., Weng, X. & Russu, I.M. Enhanced base-pair opening in the adenine tract of a RNA double helix. *Biochemistry* **50**, 1857–1863 (2011).
85. Mirau, P.A. & Kearns, D.R. Effect of environment, conformation, sequence and base substituents on the imino proton exchange rates in guanine and inosine-containing DNA, RNA and DNA-RNA duplexes. *J. Mol. Biol.* **177**, 207–227 (1984).
86. Vermeulen, A., McCallum, S.A. & Pardi, A. Comparison of the global structure and dynamics of native and unmodified tRNAval. *Biochemistry* **44**, 6024–6033 (2005).
87. Smith, F.W. & Feigon, J. Quadruplex structure of Oxytricha telomeric DNA oligonucleotides. *Nature* **356**, 164–168 (1992).
88. Cheong, C. & Moore, P.B. Solution structure of an unusually stable RNA tetraplex containing G- and U-quartet structures. *Biochemistry* **31**, 8406–8414 (1992).
89. Figueroa, N. *et al.* NMR study of slowly exchanging imino protons in yeast tRNAasp. *Proc. Natl. Acad. Sci. USA* **80**, 4330–4333 (1983).
90. Nonin, S., Jiang, F. & Patel, D.J. Imino proton exchange and base-pair kinetics in the AMP-RNA aptamer complex. *J. Mol. Biol.* **268**, 359–374 (1997).
91. Rinnenthal, J., Klinkert, B., Narberhaus, F. & Schwalbe, H. Direct observation of the temperature-induced melting process of the *Salmonella* fourU RNA thermometer at base-pair resolution. *Nucleic Acids Res.* **38**, 3834–3847 (2010).
This paper reveals enthalpy-entropy compensation in RNA base-pair opening and argues that global unfolding of an RNA thermosensor occurs when microscopic stabilities of base pairs are equalized.
92. Chen, C., Jiang, L., Michalczyk, R. & Russu, I.M. Structural energetics and base-pair opening dynamics in sarcin-ricin domain RNA. *Biochemistry* **45**, 13606–13613 (2006).
93. Dejaegere, R.A., Bryce, R.A. & Case, D.A. An empirical analysis of proton chemical shifts in nucleic acids. in *Modeling NMR Chemical Shifts* (eds., Facelli, J.C. & de Dios, A.C.) 194–206 (American Chemical Society, 1999).
94. Cromsigt, J.A., Hilbers, C.W. & Wijmenga, S.S. Prediction of proton chemical shifts in RNA. Their use in structure refinement and validation. *J. Biomol. NMR* **21**, 11–29 (2001).
95. Clore, G.M., Tang, C. & Iwahara, J. Elucidating transient macromolecular interactions using paramagnetic relaxation enhancement. *Curr. Opin. Struct. Biol.* **17**, 603–616 (2007).
96. Hansen, D.F., Vallurupalli, P. & Kay, L.E. Using relaxation dispersion NMR spectroscopy to determine structures of excited, invisible protein states. *J. Biomol. NMR* **41**, 113–120 (2008).
97. Olsen, G.L. *et al.* Solid-state deuterium NMR studies reveal mu s-ns motions in the HIV-1 Transactivation response RNA recognition site. *J. Am. Chem. Soc.* **130**, 2896–2897 (2008).
98. Wang, Y.X., Zuo, X.B., Wang, J.B., Yu, P. & Butcher, S.E. Rapid global structure determination of large RNA and RNA complexes using NMR and small-angle X-ray scattering. *Methods* **52**, 180–191 (2010).
99. Gherghe, C.M., Shajani, Z., Wilkinson, K.A., Varani, G. & Weeks, K.M. Strong correlation between SHAPE chemistry and the generalized NMR order parameter (S^2) in RNA. *J. Am. Chem. Soc* **130**, 12244–122445 (2008).
100. Sugase, K. Elucidating slow binding kinetics of a protein without observable bound resonances by longitudinal relaxation NMR spectroscopy. *J. Biomol. NMR* **50**, 219–227 (2011).